# Reservoir fracture characterizations from seismic scattered waves

*Xinding Fang\*, Mike Fehler, Zhenya Zhu, Yingcai Zheng and Daniel Burns, MIT Earth Resources Laboratory*

## SUMMARY

The measurements of fracture parameters, such as fracture orientation, fracture density and fracture compliance, in a reservoir is very important for field development and exploration. Traditional seismic methods for fracture characterization include shear wave birefringence (Gaiser and Dok, 2001; Dok et al., 2001; Angerer et al., 2002; Vetri et al., 2003) and amplitude variations with offset and azimuth (AVOA) (Ruger, 1998; Shen et al., 2002; Hall et al., 2003; Liu et al., 2010; Lynn et al., 2010). These methods are based on the equivalent medium theory with the assumption that fracture dimension and spacing are small relative to the seismic wave length, so a fracture zone behaves like an equivalent anisotropic medium. But fractures on the order of seismic wave length are also very important for enhanced oil recovery, and they are one of the important subsurface scattering sources that generate scattered seismic waves.

Willis et al. (2006) developed the Scattering Index method to extract the fracture scattering characteristics by calculating the transfer funtion of a fracture zone. Fang et al. (2011) proposed a modification of the SI method (the Fracture Transfer Function (FTF) method) that leads to a more robust fracture characterization. In this paper, we use both laboratory data and field data to explore the capability of the FTF method.

## METHODOLOGY

The transfer function of a fractured layer is expressed as (Fang et al., 2011)

$$FTF(\omega,\theta) = \frac{\left| O_2(\omega,\theta) \cdot O_1^0(\omega) \right|^{1/2}}{\left| O_1(\omega,\theta) \cdot O_2^0(\omega) \right|^{1/2} + wl} \qquad (1)$$

where $O_1(\omega,\theta)$ and $O_2(\omega,\theta)$, respectively, are the stacked data from above and below the fracture zone in azimuth $\theta$, $O_1^0(\omega)$ and $O_2^0(\omega)$ are the averages of $O_1(\omega,\theta)$ and $O_2(\omega,\theta)$ over all azimuths, $wl$ is water level.

The spatial variation of the strength of fracture scattered waves shows characteristics related to fracture spacing due to interference (Willis et al., 2005; Grandi et al., 2007; Zheng et al., 2011). Fracture scattered waves are observed to be stronger at frequencies

$$f_n = n \cdot \frac{V}{2 \cdot FS}, \quad n = 1, 2, \dots \qquad (2)$$

where $FS$ is fracture spacing and $V$ is velocity.

$f_n$ is defined as the $n$-th eigen-frequency of the fracture zone in our study, and $f_1 = \frac{V}{2 \cdot FS}$ is the base eigen-frequency. From both laboratory experiments and numerical simulations, we find that, in the direction normal to fracture strike, due to the disruptive nature of fracture scattered waves, notches can be found in $FTF$ at the eigen-frequencies after stacking, in the fracture strike direction, the scattered waves can stack con-

structively, so peaks appear at the eigen-frequencies after stacking. So the azimuthal variation of $FTF(\omega,\theta)$ is larger at the eigen-frequencies given by Equation 2. The eigen-frequencies and the azimuthal variation of $FTF$ after stacking give information about both fracture orientation and spacing.

In order to quantify the azimuthal variation of $FTF(\omega,\theta)$, which can be used to determine the fracture orientation, we define the fracture orientation function as

$$FOF(\theta) = \int_{\omega_1}^{\omega_2} FTF(\omega,\theta) \cdot SDFTF(\omega) \cdot d\omega \qquad (3)$$

with

$$SDFTF(\omega) = \sqrt{\frac{1}{N} \sum_{i=1}^{N} \left[ FTF(\omega,\theta_i) - \overline{FTF(\omega)} \right]^2} \qquad (4)$$

where $\theta$ is azimuth, $[\omega_1, \omega_2]$ is frequency window, the weighting function $SDFTF(\omega)$ is the azimuthal standard deviation of $FTF$, $\overline{FTF(\omega)}$ is the mean of the $FTF$ at frequency $\omega$, $N$ is the number of azimuthal stacks.

Because the azimuthal variation of $FTF(\omega,\theta)$ is larger at the eigen-frequencies, $FOF(\theta)$ can achieve higher resolution by preferentially choosing the data at those frequencies by adding the weighting function $SDFTF(\omega)$. The maximum of $FOF(\theta)$ gives the fracture strike direction. The frequency window $[\omega_1, \omega_2]$ should be chosen as the one that contains the scattered energy.

We want to emphasize that our analysis is based on two important assumptions: (1)azimuthal variation of the scattered energy is induced by subsurface fracture systems; (2)fracture scattered waves are preserved and enhanced if stacking is conducted along the fracture strike direction. In the following sections, we use laboratory data to explore the $FTF$ and $FOF$.

## LABORATORY EXPERIMENT

We built a parallel fracture network model by cutting parallel notches with 6.35 mm ($\pm$0.5 mm) spacing and 5 mm depth in a Lucite block, then we put this Lucite block on top of another intact Lucite block to form a two-layer model. These two Lucite blocks were coupled by a very thin water layer with thickness less than 0.5 mm, but the fractures are air-filled.

In this experiment, a P-wave source with 500 kHz central frequency and a vertical component transducer were used to generate and record seismic waves on the top surface of the model. The data were collected at 10 different azimuths. For each azimuth, 4 traces with common midpoint were collected and then stacked into a common midpoint stack after normal moveout. We only collected the data at short offset, because the scattered signals arrive at large offset are affected by the surface waves, and due to the size of transducer, we can only collect 4 traces at one azimuth.

Figure 1 shows the 10 CMP stacks corresponding to acquisitions at 10 different azimuths. For comparison, the CMP stack
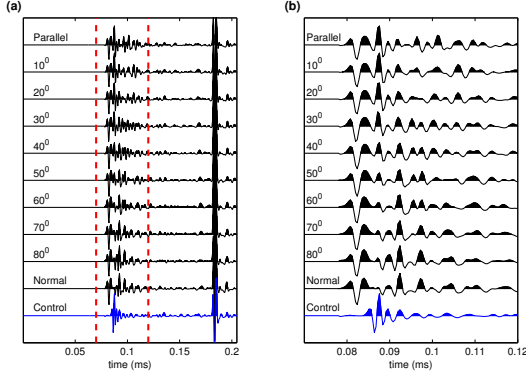
Figure 1: (a) shows CMP stacks at 10 different azimuths, (b) shows the expanded view of the waves in the red window of (a). For each azimuth, 4 traces of offsets 4 cm, 6 cm, 8 cm and 10 cm were collected and stacked at the common midpoint after applying gain and normal moveout. The acquisition angles are denoted above each trace, 'Parallel'/'Normal' indicates the acquisition is parallel/normal to the fracture strike. 'Control' represents the stack of traces collected at the region without fractures.

of 4 traces from a region without fractures is shown as the blue trace labeled 'Control'. In Figure 1, direct arrivals and surface waves have been muted, the strong signals that arrive at about 0.18 ms are the reflection from the bottom of the lower Lucite block, the signals inside the red window are the waves scattered from the fracture zone.

Because there is no layer interface above the fracture zone in the Lucite model, we compute the $FTF$, which is shown in Figure 2, by using the Control trace to estimate the reflectivity of the interface between the two Lucite blocks. In our analysis, the analysis time window length is 0.05 ms and time sampling is $0.4 \times 10^{-6}$ s, so the frequency resolution is 20.2 kHz. A higher frequency resolution can be obtained by increasing the length of the time window, however, the window length is restricted by our Lucite model, because the results will be influenced by the P-to-S converted waves from the interface and the surface waves if a longer window is chosen. Because stacking at different azimuths has different effects on the fracture scattered waves, so the $SDFTF(\omega)$, which is shown as the magenta curve in Figure 2, has a larger value at the eigenfrequency which can be predicted by Equation 2. From Figure 2, we can clearly see the eigen-frequencies correspond to the numbering of $n=2$ and 3. The white error bars show the uncertainties of the predicted eigen-frequencies induced by the error of fracture spacing ($\pm$0.5 mm). For $n=1$, the corresponding eigen-frequency shown from the data shifts toward higher frequency comparing to the predicted value, this is caused by the insufficient fold in stacking.

For the $FTF$ at frequency $< 200$ Hz, the value at $90^0$ (normal to fracture strike) is higher than that at $0^0$ (parallel to fracture strike), which seems to be conflicting with our statement on the characteristic of azimuthal stacking of fracture scattered
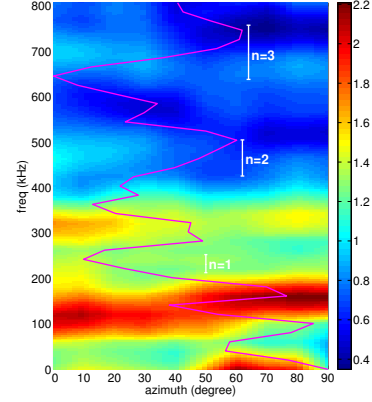


Figure 2: Plot of the $FTF$ of the fracture zone. $0^0$ and $90^0$ at X-axis represent the direction parallel and normal to the fracture strike, respectively. The magenta curve shows the normalized $SDFTF$ (log scale). The numbers $n$ in the figure are the numbering of the eigen-frequencies predicted by Equation 2. White error bars show the uncertainties of each eigen-frequency.

waves. To explain this, instead of using the scattering theory, it would be more appropriate to adopt the effective medium theory. From traditional AVOA analysis (e.g. Ruger (1998)), which is based on the effective medium theory, we know that the amplitude of the reflected waves from above a fracture zone is larger if the wave propagation direction is normal to the fracture strike direction, which has higher impedance contrast. The analysis time window chosen for computing the $FTF$ already contains these reflected waves from the fracture zone, which are the waves that arrive at about 0.08 ms in Figure 1. Therefore, the analysis window includes both scattered waves and the reflected waves which have the AVAZ characteristics. In Figure 2, the $FTF$ at high frequency ($>$200 kHz) agrees with our understanding on fracture scattering, and the $FTF$ at low frequency ($<$200 kHz) agrees with the effective medium theory. The value of the $FTF$ below 100 kHz may not be reliable, because the source has little energy in this frequency range and spurious high amplitude could be caused by the spectral division.

In Figure 3, the fracture orientation can be clearly determined from the variation of $FOF$ (solid curve), which is defined by Equation 3. Because the central frequency of the source is 500 kHz, so 200kHz-800kHz would be a reasonable frequency window for computing the $FOF$. The fluctuation of $FOF$ near the normal direction is caused by the low fold in stacking. For comparison, we also show the sum of $FTF$ without adding the weighting function $SDFTF(\omega)$. In Figure 3, we can see that a higher directional resolution can be obtained by adding the weighting function in Equation 3.

## APPLICATION TO THE EMILIO FIELD

Multi-azimuth data were collected over the Emilio Field, which is near the eastern coast of Italy, through a 3D/3C seismic sur-
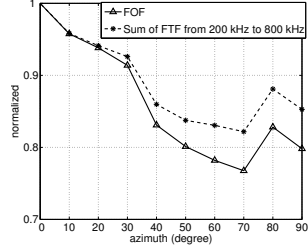
Figure 3: Solid curve shows $FOF$ defined by Equation 3, the frequency window in the calculation is from 200 kHz to 800 kHz. Dash curve is the sum of $FTF$ in the same frequency window without adding the weight.
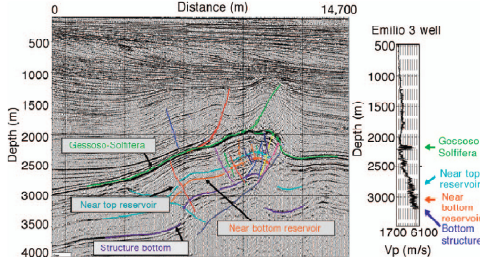


Figure 4: Profile through the Emilio PP data showing the interpreted seismic section (left) and the interval velocity log (right). The reservoir top and bottom are, respectively, marked by the cyan and amber curves. (Adapted from Willis et al. (2006)).
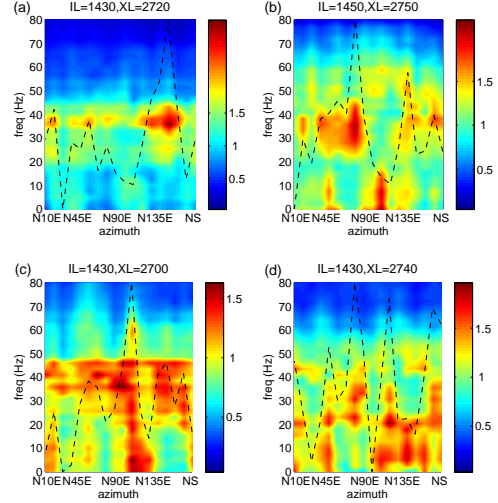


Figure 5: $FTF$ at four different CDP locations. The inline and crossline numbers of each CDP are shown on top of each panel. Horizontal axes represent azimuth, N10E indicates north $10^0$ to east, NS indicates north-south. Black dash curves are the normalized $FOF$.

$$Con = \frac{\sqrt{\frac{1}{N}\sum_{i=1}^{N}\left[FOF(\theta_i) - \overline{FOF}\right]^2}}{\overline{FOF}} \quad (5)$$

where $\overline{FOF}$ is the mean of $FOF$, and $N$ is the total number of azimuths.

By definition (equation 5), small angular contrast in $FOF$ represents low confidence on fracture orientation detection, in other words, larger angular contrast gives us higher confidence on the measurements. We perform model smoothing of the directions and confidences in Figure 6 by using a 400 m × 400 m box centered at each CDP. Following Willis et al. (2006), the fracture direction for each CDP location is chosen as the one which most frequently occurs in the 400 m × 400 m box of CDPs around it. The confidence is taken as the average confidence of those CDPs giving the fracture direction that most frequently occurs in the smoothing box. Comparing our result with the SI method of Willis et al. (2006) and the PS anisotropy method of Vetri et al. (2003), we find that these three results, which are derived from three different methods, give the similar fracture orientation trends.

From the analysis of the our laboratory experiment, we know that the $SDFTF$ can be used to estimate the fracture spacing, and Equation 3 gives the relationship between fracture spacing and the $FTF$. Figure 7 shows two slices of the $SDFTF$ at Inline 1450 (Figure 7a) and Crossline 2770 (Figure 7b). In these two figures, most of the high amplitude peaks (warm color), which indicate eigen-frequencies, appear between 20 Hz and 60 Hz. The spurious high values near 0 Hz are induced by the spectral division. The $SDFTF$ at each CDP may have several peaks corresponding to different orders of eigen-frequency, however, we still do not know how to determine the corresponding order 'n' of each eigen-frequency. From

vey in early 2000. In 2006, Willis et al. created 18 stacked CDP volumes from the vertical-component data by stacking the near-to-mid-range (<3500 m) offsets of the preprocessed PP data in 18 different azimuth orientations from east to west in $10^0$ steps with $20^0$-wide overlapping ranges. Figure 4 shows the interval velocity log and one interpreted seismic section through the field. The Gessoso-Solfifera highlighted in green in Figure 4, which is interpreted as a high-velocity chalk formation, is the strongest reflector that can be easily recognized from the seismic data. The reservoir interval, which is shown between the cyan and amber curves on the seismic section, is at about 2800 m depth, and its thickness is a few tens of meters.

The $FTF$ at 18 different azimuths is computed at each CDP location. Figure 5 shows the $FTF$ and the corresponding $FOF$ at four different CDP locations. In Figures 5a and 5b, the $FOF$ (black dash) curves clearly indicate that fractures are orientated at $N150^0E$ and $N80^0E$ at these two locations. The two red spots at about 35 Hz give information about fracture spacing. The $FTF$ in Figures 5c and 5d are vague, this results in ambiguity on the detection of fracture direction, but we still can use the maximum of $FOF$ to find the dominant fracture direction.

Figure 6a plots the fracture directions for all CDP locations and 6b shows the confidence of the measurements, which is defined as
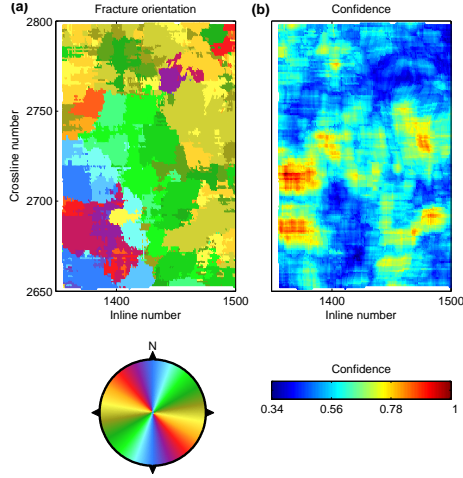
Figure 6: (a) is the map of fracture orientation at reservoir depth, the color hue indicates the direction of detected fractures and the color legend is shown right below the figure. (b) is the confidence, which is defined in Eqation 5, of fracture direction detection, warn color represents high confidence and cold color represents low confidence, confidence is normalized to 1 in plotting. The time window for computing the $FTF$ is 400 ms, and the frequency window for calculating the $FOF$ is from 20 Hz to 70 Hz.

the velocity log, we know that the average P-wave velocity of the formation above the reservoir is about 2500 m/s in the Emilio Field. The FMI logs show that the fracture spacing varys from 10 m to 50 m, this implies that the base eigen-frequencies vary from 25 Hz to 125 Hz. A fracture system with too small fracture spacing ($<$ 20 m) can not be resolved by our approach, other methods, such as AVOA, have to be used to study these dense fracture networks. Generally, the fracture spacing of a fractured reservoir is on the order of the reservoir interval thickness, which is a few tens of meters in the Emilio Field. That means the base eigen-frequencies of the fracutre zone should between 25 Hz and 125 Hz. Most peaks shown in Figure 7 are between 20 Hz and 60 Hz. At each CDP, we assume that the $SDFTF$ has the maxima at the base eigen-frequency in this frequency range. Then we use Equation 3 to compute the fracture spacing. Figure 8a shows the variation of the fracture spacing at the reservoir depth in the Emilio Field. Figure 8b shows the fracture spacing smoothed by using a 400 m $\times$ 400 m box centered at each CDP. From Figure 8a, we can see that the fracture spacings obtained from the $SDFTF$ are not randomly distributed, they show a variation pattern, which is much clearer after smoothing, as shown in Figure 8b. The result is promising, but we still need to find a better way to determine the base eigen-frequency and to develop an uncentainty analysis for fracture spacing.

## CONCLUSIONS

The $FTF$ provides a means to measure the azimuthal variation of seismic scattering at each CDP. By applying Equa-
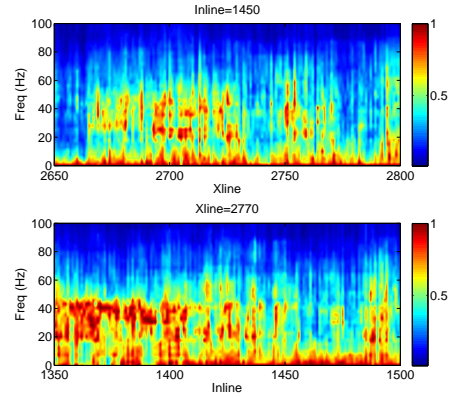


Figure 7: (a) and (b) show two profiles of the $SDFTF$ at Inline 1450 and Xline 2770, respectively. The $SDFTF$ at each CDP is normalized to 1.
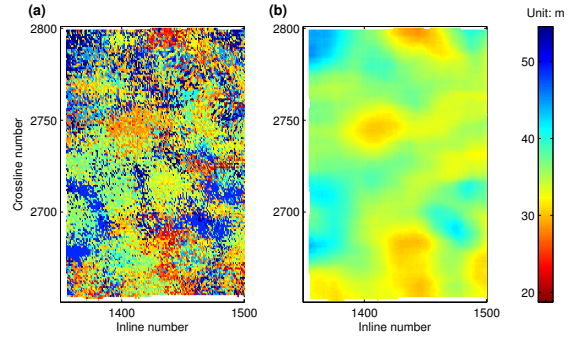


Figure 8: (a) shows the distribution of fracture spacing obtained by picking the peak of the $SDFTF$ at each CDP and (b) shows the fracture spacing smoothed by a 400 m $\times$ 400 m box.

tions 2 and 3, the fracture orientation and fracture spacing can be determined from the $FTF$. Our approach has been tested using laboratory experiment data. The application of this method at the Emilio Field provides information about both fracture orientation and fracture spacing. The $FTF$ derived fracture orientation agrees with the results obtained from the SI method (Willis et al., 2006) and PS anisotropy study (Vetri et al., 2003). Compared to the SI method, the advantage of this approach is its robustness. We find that we can obtain a stable and accurate result from the $FTF$. However, our approach can only be applied to a fracture network with the fracture spacing on the order of seismic wavelength. For fracture spacing estimation, we still need to find a better way to determine the base eigen-frequency and to develop an uncertainty analysis method.

## ACKNOWLEDGMENTS

**REFERENCES**

Angerer, E., S. A. Horne, J. E. Gaiser, R. Walters, S. Bagala, and L. Vetri, 2002, Characterization of dipping fractures using ps mode-converted data: SEG Technical Program Expanded Abstracts, **21**, 1010–1013.

Dok, R. V., J. Gaiser, and J. Markert, 2001, Green river basin 3-d/3-c case study for fracture characterization: Common-azimuth processing of ps-wave data: SEG Technical Program Expanded Abstracts, **20**, 768–771.

Fang, X., M. Fehler, Z. Zhu, T. Chen, and D. Burns, 2011, A robust method for fracture orientation and density detection from seismic scattered energy: Annual Sponsors' Meeting of the Massachusetts Institute of Technology Earth Resources Laboratory.

Gaiser, J., and R. V. Dok, 2001, Green river basin 3-d/3-c case study for fracture characterization: Analysis of ps-wave birefringence: SEG Technical Program Expanded Abstracts, **20**, 764–767.

Grandi, S., M. Willis, D. Burns, and M. Toksoz, 2007, Analysis of scattered signal to estimate reservoir fracture: Annual Sponsors' Meeting of the Massachusetts Institute of Technology Earth Resources Laboratory.

Hall, S., J. Kendall, et al., 2003, Fracture characterization at Valhall: Application of P-wave amplitude variation with offset and azimuth (AVOA) analysis to a 3D ocean-bottom data set: Geophysics, **68**, 1150.

Liu, E., G. Zelewski, C.-P. Lu, J. Reilly, and Z. J. Shevchek, 2010, Seismic fracture prediction using azimuthal avo analysis in a middle east carbonate field: workflow and mitigation of overburden effects: SEG Technical Program Expanded Abstracts, **29**, 268–272.

Lynn, H., S. R. Narhari, S. Al-Ashwak, V. K. Kidambi, B. Al-Qadeeri, and O. Al-Khaled, 2010, Pp azimuthal-amplitudes and -acoustic impedance for fractured carbonate reservoir characterization: SEG Technical Program Expanded Abstracts, **29**, 258–262.

Ruger, A., 1998, Variation of P-wave reflectivity with offset and azimuth in anisotropic media: Geophysics, **63**, 935.

Shen, F., J. Sierra, D. Burns, and M. Toksoz, 2002, Azimuthal offset-dependent attributes applied to fracture detection in a carbonate reservoir: Geophysics, **67**, 355.

Vetri, L., E. Loinger, J. Gaiser, A. Grandi, and H. Lynn, 2003, 3D/4C Emilio: Azimuth processing and anisotropy analysis in a fractured carbonate reservoir: The Leading Edge, **22**, 675.

Willis, M., D. Burns, R. Rao, B. Minsley, M. Toksoz, and L. Vetri, 2006, Spatial orientation and distribution of reservoir fractures from scattered seismic energy: Geophysics, **71**, O43.

Willis, M., R. Rao, D. Burns, and M. Toksoz, 2005, Fracture spacing and orientation estimation from spectral analysis of azimuth stacks: Annual Sponsors' Meeting of the Massachusetts Institute of Technology Earth Resources Laboratory.

Zheng, Y., X. Fang, M. Fehler, and D. Burns, 2011, Double-beam stacking to infer seismic properties of fractured reservoirs: SEG Technical Program Expanded Abstracts, **30**, 1809–1813.